Geophys. J. Int. (2008) **174,** 567–584 doi: 10.1111/j.1365-246X.2008.03791.x

Geophysical characterization of the Ota–Vila Franca de Xira–Lisbon–Sesimbra fault zone, Portugal

João Carvalho,[1] Taha Rabeh,[2] João Cabral,[3] Fernando Carrilho[4] and Jorge Miguel Miranda[5]

[1] *Instituto Nacional de Engenharia, Tecnologia e Inovação, Estrada da Portela – Zambujal,* 2720-461 *Amadora, Portugal. E-mail: joão.carvalho@ineti.pt*
[2] *National Research Institute of Astronomy and Geophysics, Helwan, Cairo, Egypt*
[3] *LATTEX, IDL, Ed. C6, 2° Piso, Campo Grande,* 1749-016 *Lisboa, Portugal*
[4] *Instituto de Meteorologia, Av. do Aeroporto,* 2300-313 *Lisboa, Portugal*
[5] *University of Lisbon, CGUL, IDL. Campo Grande,* 1749-016, *Lisboa, Portugal*

Accepted 2008 March 14. Received 2008 February 12; in original form 2006 November 29

SUMMARY

This paper focuses on the reprocessing of seismic reflection profiles, aeromagnetic and seismicity data, to locate and characterize the Ota–Vila Franca de Xira–Lisbon–Sesimbra fault zone. The studied structure is sited in the Lower Tagus Valley, an area with over 2 million inhabitants, that has experienced historical earthquakes causing many casualties, serious damage and economical losses (e.g. 1531 January 26 and 1909 April 23 earthquakes), whose tectonic sources are mostly unknown. The fault zone trends NNE–SSW to N–S, is located near the eastern border of the Mesozoic Lusitanian Basin and partially delimits the Lower Tagus Cenozoic Basin at the west, mostly hidden under the Cenozoic sedimentary fill. According to the data presented here, the normal structures that compose the fault zone were reactivated in Cenozoic times, with positive inversion and the development of splays towards the east. The fault zone shows three distinct segments with different behaviour, in conformity with their various orientations relative to the NW–SE maximum compressive stress. The northern segment splays into a series of NNE–SSW oriented, east verging, imbricate thrusts, which merge to the west into a major reverse fault that resulted from the tectonic inversion of the former normal fault bordering the Mesozoic Lusitanian Basin in this area—the well known Ota (or Pragança) fault. The central segment corresponds to the approximately 20 km long outcropping Vila Franca de Xira fault, which suffered a maximum degree of inversion. The southern segment extends for ∼45 km, crossing Lisbon and the Setúbal Península at depth until approximately Sesimbra (probably continuing offshore), with an N–S trend and distinct geometry. South of Vila Franca de Xira, there is evidence for a WSW–ENE fault located at depth, producing a righ-lateral stepover on the major structure and splitting the central from the southern segment. We hypothesize that this obliquely trending fault is a possible source of the 1909 Benavente earthquake.

Key words: Magnetic anomalies: modelling and interpretation; Seismicity and tectonics; Acoustic properties; Continental neotectonics; Fractures and faults.

1 INTRODUCTION

Our study area is located in central Portugal mainland (Fig. 1) and experiences an earthquake activity that presents a significant threat for this densely populated metropolitan Lisbon area, stressing the need to identify and characterize regional seismogenic faults as a condition for seismic potential assessment. Due to the thickness of the sedimentary cover, many of the active and/or potentially active regional tectonic structures can only be studied through geophysical methods. Therefore, reprocessing and reinterpretation of seismic reflection data acquired for oil exploration in the Lower Tagus Valley (LTV) and surrounding areas is presented here in an attempt to improve knowledge regarding the deep structure, in particular the location and characterization of hidden faults, which may be the source of the regional seismicity (Cabral *et al.* 2003; Carvalho *et al.* 2006).

Available seismic data reach at most 4–5 km depth, allowing the location and characterization of structures in the Cenozoic and Mesozoic rocks, but they do not image the faults inside the Palaeozoic basement. To locate the faults deep in the basement and improve the correlation between faults and earthquakes, potential-field data can be used. For this purpose, reprocessing and reinterpretation of aeromagnetic data collected in 1969 by Fairey Surveys were carried out.

The Ota–Vila Franca de Xira–Lisbon–Sesimbra (OVLS) fault zone consists of a set of aligned and interrelated NNE–SSW to N–S

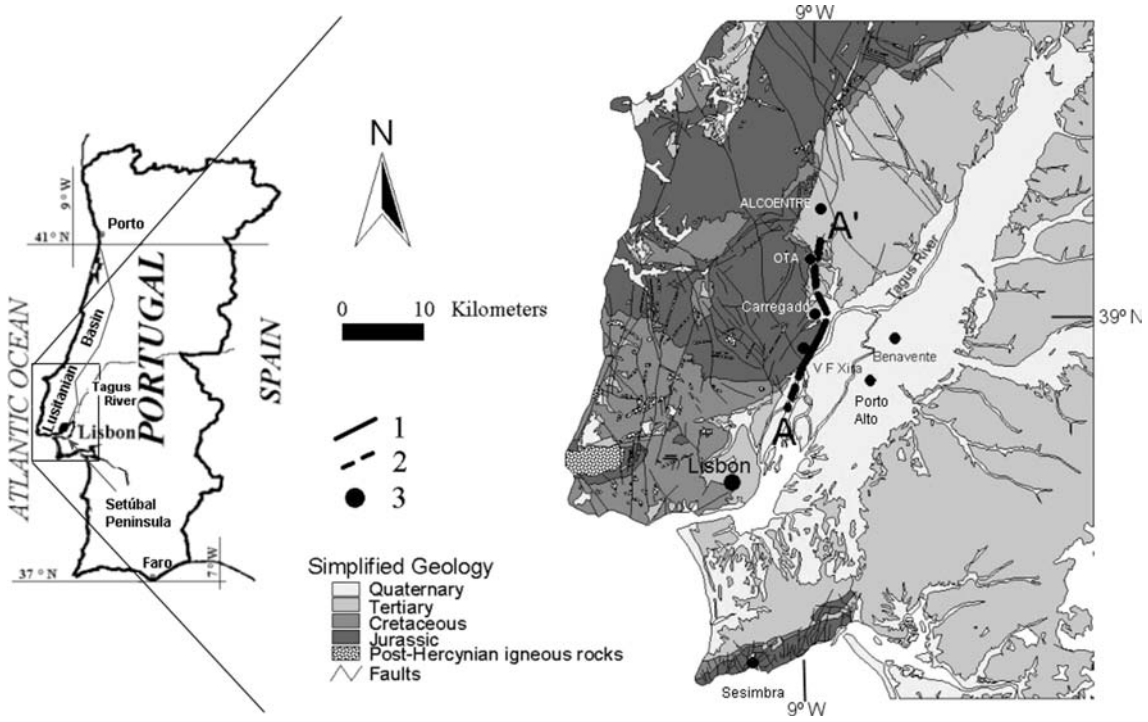

Figure 1. Location map and simplified geology (after Oliveira *et al.* 1992) of the study area. A-A′ – Ota and Vila Franca de Xira segments of the OVLS fault zone; 1 – outcropping fault zone near Vila Franca de Xira; 2 – fault zone after the seismic reflection profiles interpretation and 3 – localities mentioned in the text.

trending faults, extending along the western border of the Lower Tagus Cenozoic Basin (LTCB) from approximately the Montejunto massif (Fig. 2) at the north to Sesimbra at the south. It was selected as a priority target for further investigation, based upon its near-surface expression on the seismic reflection profiles at some locations, its significance in the LTCB structural pattern and apparent relationship with the regional seismicity, its closeness to Lisbon and its foreseen seismic potential. This work discusses the interpretation and analysis of recently reprocessed geophysical data mentioned above (seismic reflection profiles, aeromagnetic data and seismicity data) to achieve a better characterization of this fault zone.

The study area is located roughly 150–200 km north of the Iberia–Africa plate boundary (the Azores–Gibraltar fracture zone) and has suffered the effects of large historical earthquakes, which caused severe damage and many casualties. The seismic activity comprises relatively distant events, as the 1755 November 1 earthquake, one of the largest historical earthquakes ever described (estimated magnitude $\geq$8.5; Martins & Mendes-Victor 1990). The 1755 event was probably generated by N–S to NNE–SSW trending offshore structures located southwest of the Portuguese coastline (Zitellini *et al.* 1999, 2001; Baptista *et al.* 2003; Gràcia *et al.* 2003).

Besides the effects of the earthquakes generated in the southwestern offshore area, directly connected to the Iberia–Africa plate boundary, the study region experiences a significant intraplate seismicity, attested by the occurrence of moderate to large local historical earthquakes, as in 1344, 1531 and 1909, with estimated magnitudes ranging from 6 to 7 (Mezcua 1982; Moreira 1984, 1985; Oliveira 1986; Martins & Mendes-Victor 1990; Justo & Salwa 1998). Due to the scarcity of historical descriptions, the earthquakes in 1344 and 1531 are poorly located, being positioned in the LTV based upon the destruction generated in the Lisbon area. The 1531 event caused severe damage and many casualties in the town of Lisbon, reaching an intensity of VIII–IX MM (Justo & Salwa 1998).

The source of the $M_W = 6$ ($M_S = 6.3$) 1909 earthquake (Teves-Costa *et al.* 1999; Dineva *et al.* 2002), which destroyed the village of Benavente (Fig. 1), is still unknown. The OVLS fault zone, or the southern, hidden sector of the Azambuja fault (Fig. 2) are the nearest, NNE–SSW trending, candidates (Cabral *et al.* 2003, 2004; Carvalho 2003). An alternative, as proposed by Stich *et al.* (2005), is that the Benavente earthquake was generated by an ENE–WSW trending blind thrust beneath the Tagus valley sedimentary basin. This conclusion was drawn from the moment tensor inversion solution, which indicated almost pure reverse faulting with nodal planes oriented (051°, 52° SE) and (242°, 38° NW) (Stich *et al.* 2005) Later in this paper, we will propose a fault with compatible characteristics.

The importance of local seismic sources to the seismic hazard of the LTV area has been recently pointed out by many authors (e.g. Peláez *et al.* 2002; Cabral *et al.* 2003, 2004; Vilanova *et al.* 2003; Vilanova & Fonseca 2004; Carvalho *et al.* 2006). However, the low instrumental seismicity, as a consequence of the small slip rate, the poor earthquake location due to the sparse national network and the presence of a thick sedimentary cover, does not show a clear relationship between the earthquakes locations and mechanisms and the faults recognized at the surface. The geometry and topography of the Tertiary and Mesozoic sedimentary basins also play an important role on local energy enhancement and site-effects, masking the relationship between the historical events location based on seismic intensity studies and the earthquake sources. We propose that the OVLS fault zone is responsible for most of the instrumental seismicity registered in the study area.

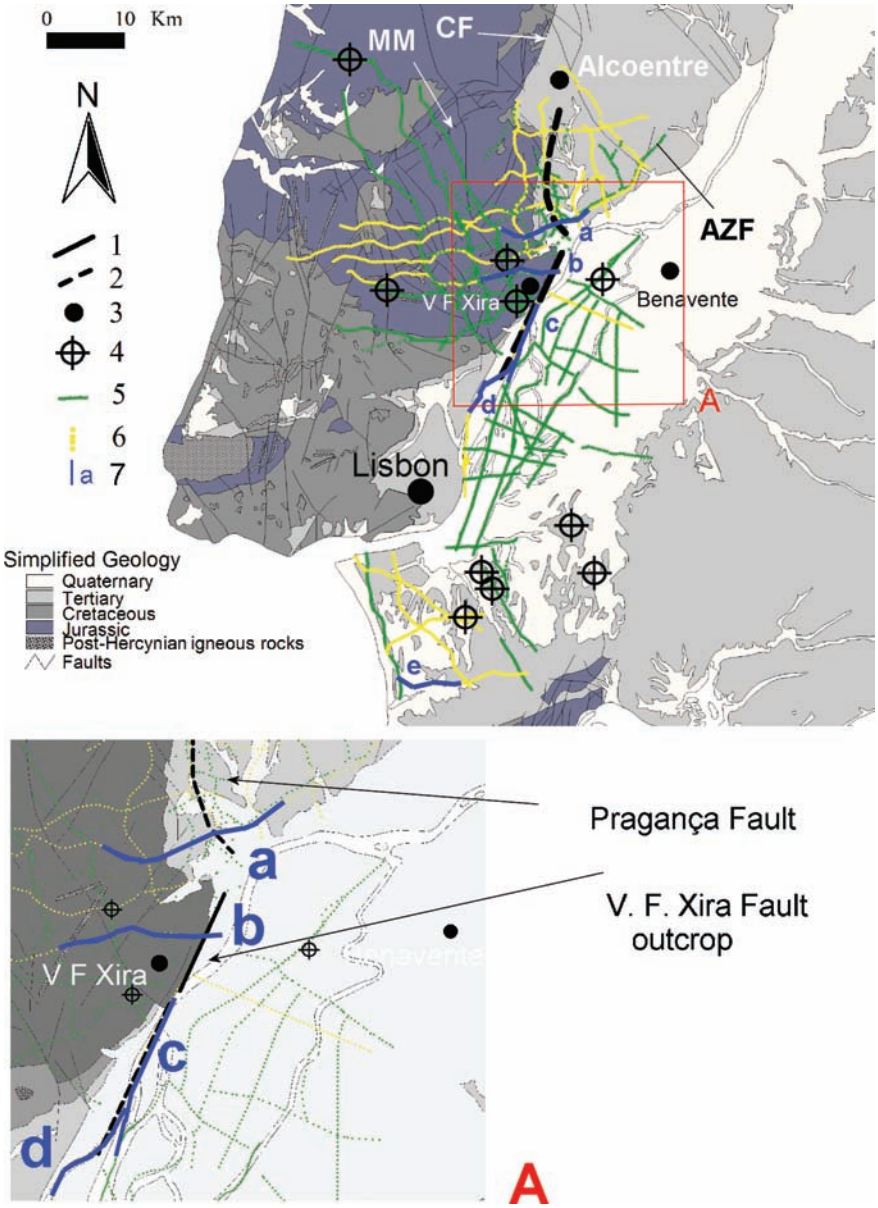

Figure 2. Used seismic and well data overlaid on a simplified geological map (after Oliveira *et al.* 1992). 1 – outcropping fault zone near Vila Franca de Xira; 2 – extent of the fault zone after Carvalho (2003); 3 – localities mentioned in the text; 4 – deep wells; 5 – oil industry seismic reflection profiles used for structural mapping of the Lusitanian and Lower Tagus basins; 6 – seismic-reflection profiles used in this work to study the OVLS fault zone. 7 – seismic profiles shown in Fig. 3. CF – Cercal fault; AZF – Azambuja fault; MM – Montejunto massif.

2 GEOLOGICAL SETTING

The study area includes part of the LTCB, a tectonic depression filled with Cenozoic sediments that surrounds the lower reach of the Tagus River, and the Arruda subbasin, which is part of the Mesozoic Lusitanian Basin (LB) (Fig. 1). A brief description of the former basin can be found in Cabral *et al.* (2003) whereas the evolution of the latter basin is described in Leinfelder & Wilson (1998), Rasmussen *et al.* (1998), Carvalho *et al.* (2005) and others.

Several outcropping faults affect the LB whereas a few affect the LTCB sediments. From geophysical data several other non-outcropping fault zones were mapped in the LTCB (Cabral *et al.* 2003; Carvalho *et al.* 2006). For some of them, such as the Vila Fanca de Xira, Azambuja, Pinhal Novo and Porto Alto faults, there is evidence of tectonic activity since the Pliocene (Cabral *et al.* 2003; Carvalho *et al.* 2006).

The OVLS fault zone consists of a set of NNE–SSW to N–S trending, deep seated fault segments, located near the western border of the LTCB. It comprises three main segments, mostly hidden under the Cenozoic sedimentary cover (particularly the recent alluvial sediments of the Tagus River). The northern and central segments behaved in the Mesozoic as normal faults flanking the LB in this area and were inverted under the action of a NW oriented maximum compressive stress in the Cenozoic. The southern sector reacted differently to the regional compression, suffering minor inversion.

The northern segment of the fault zone corresponds to the N–S to NNE–SSW trending Ota (or Pragança) fault, which extends for ∼20 km from north of Ota to near Carregado, at the south

(Fig. 1 for locations). It is represented at the surface by an east dipping monocline, affecting the Tertiary sediments of the LTCB. The central segment corresponds to the partially outcropping Vila Franca de Xira fault, which extends for another ∼20 km to the SSW of Carregado (Fig. 1), being probably interrupted by a deep WSW–ENE fault located north of Lisbon. This segment suffered the maximum degree of tectonic inversion in the Cenozoic. The southern segment of the OVLS fault zone extends for ∼45 km, crossing Lisbon and the Setúbal Península at depth until approximately Sesimbra (probably continuing offshore) with an N–S trend and distinct geometry. It was barely inverted in the Cenozoic and is scarcely expressed on the surface geology, where Neogene sediments predominate, its presence at depth being inferred from the studied geophysical data.

Among the three segments of the OVLS, Vila Franca de Xira segment is better exposed on the surface geology. It consists of a NNE–SSW trending complex, known from surface geology and geophysical data (Domzalski 1969). It was generated in the Mesozoic as a large normal fault, bounding at the East the Arruda halfgraben of the LB (Rasmussen *et al.* 1998), later tectonically inverted and moving with reverse slip component during the Neogene.

This segment of the fault zone is partially hidden under recent alluvium of the Tagus river plain along most of its length. For 5 km southward of Vila Franca de Xira, it outcrops as a steeply dipping reverse fault, thrusting Jurassic rocks of the LB at the west, over tilted Upper Miocene sediments of the LTCB, at the east. To the south, it is intersected by a transverse NW–SE fault system (probably the Porto Alto fault system of Carvalho *et al.* 2006) and is apparently offset eastwards under the sediments of the Tagus alluvial plain through a left-lateral stepover.

The extension of this segment of the OVLS fault zone further south, as a blind thrust under the recent alluvia of the Tagus river plain, is suggested by the eastwards dipping monocline that affects the Tertiary sediments in this area. Geophysical data also show the presence of an eastward dipping monocline and of a fault at depth near the western bank of the Tagus river, south of Vila Franca de Xira (Domzalski 1969; Walker 1983; GPEP 1986; Carvalho *et al.* 2006).

On its northern side, the extension of the fault zone a few kilometres northwards of Vila Franca de Xira is indicated by the presence of outcropping faults affecting Jurassic rocks, and it is also suggested by data from several oil-industry seismic profiles, where a few authors have interpreted a series of thrust faults as an imbricate system, merging at the main inverted normal fault to the west (Lomholt *et al.* 1995; Cabral *et al.* 2003; Carvalho *et al.* 2006). However, due to a gap in the seismic lines, the link between any of these faults to the Vila Franca de Xira fault segment cannot be clarified.

Although the fault zone shows a significant geomorphic expression in this sector, particularly near Vila Franca de Xira, where it is located along a steep slope at the western bank of the Tagus estuary, no clear evidence of fault displacements affecting the Holocene alluvial deposits have been found so far (Carvalho *et al.* 2006). This may be due to the low fault slip rate and the high river dynamics which can easily obliterate (erode and/or bury) any evidence of recent surface faulting. Nevertheless, shallow geophysical data acquired recently suggests a vertical offset of about 5 m in Holocene sediments (Carvalho *et al.* 2006).

3 INTERPRETATION OF THE SEISMIC REFLECTION PROFILES

3.1 Seismic reflection data reprocessing

The study area has partially been covered by seismic reflection data acquired by the oil-industry from the 1950s to 1982 (see Table 1). Due to advances in processing software and computing, reprocessing of this information was expected to provide an enhanced imaging of the profiles. Therefore, over 60 seismic reflection profiles, corresponding to more than 800 km (Fig. 2), were reprocessed and reinterpreted. A part of this data set was used to study the tectonic and sedimentary evolution of the LB (Carvalho *et al.* 2005) and for a better evaluation of the seismic potential of the study zone (Carvalho *et al.* 2006).

In this study, additional lines in the Setúbal Peninsula were reprocessed and reinterpreted by the authors. Unpublished data, processed by Fairfield Industries in the right-hand margin of the Tagus (courtesy of Mohave Oil), were also used. The complete data set is summarized in Table 1. The details of the reprocessing can be found in Table 2. All migrated stacked sections are of better quality than the original ones. The frequency content of the migrated stacks from all the surveys is in the range of about 12–50 Hz. Depth conversion was applied to all profiles, using the layer cake method (Marsden 1989) with a velocity gradient for each layer, similarly to Jaspen (1993) methodology, but without velocity anomalies, since they may introduce false structures due to sparse well control.

3.2 Data interpretation

Several well logs and synthetic seismograms, VSP, aeromagnetic and gravimetric reprocessed data were used in the reinterpretation of the seismic profiles, as well as recent geological information (Carvalho *et al.* 2005). All these data were georeferenced and integrated in a GIS environment. After the identification by Carvalho *et al.* (2006) of major structures affecting the upper

Table 1. Seismic acquisition parameters of the different seismic reflection surveys used in this work.

Seismic survey	Contractor	Date	Offsets (m)	Seismic source	Nominal fold
Tejo	Geco-Prakla	1978	100–1250	Air-gun	24
Samora	CGG	1979	100–2450	Vibroseis	24
Arruda CPP	Prakla-Seismos	1954-1955	20–240	Dynamite	1
Arruda 80	CGG	1980	100–1250	Vibroseis	24
Arruda 81	CGG	1981-1982	120–1530	Vibroseis	24
Barreiro	CGG	1963	100–2450	Vibroseis	24
Bombarral	Quest Party	1979	450–1600	Geosel	12
Caparica	CGG	1981	120–1530	Vibroseis	24

Note: The surveys from Arruda were recently reprocessed by Fairfield Industries using pre-stack time migration (courtesy of Mohave Oil). All other surveys were reprocessed by the authors, except profile C6 from the Caparica survey, which was kindly reprocessed by DECO Geophysical.

Table 2. Principal steps applied in the processing of the seismic reflection data.

Processing step	Parameters used
Butterworth passband	15–250 Hz, 18dBoct^{-1}
Spherical divergence	Time^2 × velocity^2
Mute	First arrivals
Elevation and refraction statics	Velocity models obtained from original sections
Deconvolution	Prediction length:10 ms, operator length: 250 ms
Velocity analysis	Constant velocity panels
Residual statics	Maximum allowable shift 8 ms
Velocity analysis	Constant velocity panels
DMO	FK DMO
Velocity analysis	Constant velocity panels
NMO correction+stack	Stretch mute 70 per cent
Phase-shift migration	Interval velocities
Post-stack processing	Time-variant butterworth, amplitude equalization, spatial noise filter

Note: The Arruda 80 and 81 surveys were reprocessed by Fairfield Industries, using pre-stack time migration.

Neogene, several stacked sections were selected for a detailed study of the OVLS fault zone (Fig. 2). The faults were identified by visual inspection of the stacks using seismic attributes, by verifying fault consistency from line to line and the observation of 3D horizon structural maps. Potential field data were plotted over the seismic profiles and used to confirm major faults in the Mesozoic and Palaeozoic rocks, as well as other geological structures. Further profiles and surveys than the ones studied by Carvalho *et al.* (2005, 2006) were included in this work to enlighten the north and southwards prolongation of the fault zone. Fig. 3 shows the OVLS fault zone in several seismic profiles.

Evidence of the fault zone at its northern sector, south of Alcoentre (see Fig. 1 for location) can be seen in a series of faults with different geometries affecting the Meso-Cenozoic and Palaeozoic cover. The deformation of the Mesozoic and Cenozoic sedimentary cover produced by this fault segment is also apparent in seismic profiles located further south, as in the example shown in Fig. 3(a) (see Fig. 2 for location).

In its sector near Vila Franca Xira, the OVLS fault zone presents a greater degree of inversion, as evidenced in seismic section of Fig. 3(b). This section is consistent with the statement by Carvalho *et al.* (2006) that near the western bank of the Tagus river, the Jurassic rocks rapidly drop from the surface to a depth of more than 300 m.

One or two kilometres south of Vila Franca Xira, the seismic lines available have a strike subparallel to the fault itself, making them barely suitable for studying this structure. The undulated geometry of the reflectors in the seismic sections located to the south of section in Fig. 3(b) (Figs 3c and d) is due to distinct causes, where the interference of the OVLS fault zone is difficult to recognize.

In the section of Fig. 3(c), the occurrence of a thick Cenozoic sedimentary sequence (0.5–1.5 km) along the profile suggests that it is located on the footwall of the Vila Franca de Xira fault segment, which probably passes immediately to the west of the profile. In fact, surface geology (Zbyszewski *et al.* 1981) shows that Jurassic sediments outcrop only 250 m west of central part of the profile. The observed folding and faulting of the seismic horizons is probably produced by a partially mapped NW–SE transfer fault (Zbyszewski *et al.* 1981), which intersects and laterally offsets the OVLS fault zone in this area.

The profile shown in Fig. 3(d), located to the south of the previous profile, curves towards the west and intersects a fault zone that has different characteristics. The vertical offsets are small, and the observed geometry across the Cenozoic sediments suggests a prevailing strike-slip behaviour in this area. The folding observed in Fig. 3(d) partially results from a change in the trend of the seismic section relatively to the strike of the sedimentary sequence.

South of the location of the profile shown in Fig. 3(d), the OVLS fault zone is not recognized in the stacked seismic sections available, which are oriented approximately E–W. The analysis of the aeromagnetic data (see Section 4) indicates that it bends westwards south of Fig. 3(d). This may explain the different characteristics of the fault zone detected in Fig. 3(e), which possibly corresponds to the southern termination of the OVLS fault segment located to the north. This suggests that this structure is probably segmented in this area, and we shall see in the following discussion that it is most likely due to a WSW–ENE trending fault that locally offsets the OVLS fault zone.

According to the interpretation of aeromagnetic data (presented in the Section 4), the fault zone bends towards the west and then acquires a N–S trend, crossing at depth the area of the city of Lisbon and continuing south, into the Setúbal Península. Another seismic reflection survey acquired in 1981 in this southern area was therefore reprocessed and reinterpreted to confirm the fault zone location according to the aeromagnetic data. Fig. 3(e) shows a stacked section in this area. The fault zone is recognized in this seismic section as a set of two nearly vertical faults affecting the Mesozoic and Palaeozoic units, though some deformation also affects the Cenozoic layers. The seismic data, therefore, supports the southern prolonging of the OVLS fault zone into the Setúbal Península although with different geometry and kinematics.

4 AEROMAGNETIC DATA INTERPRETATION

The aeromagnetic data was acquired during 1969 by Fairey Surveys Limited throughout the Portuguese Atlantic margin. The altitude of the flight was 600 m, with flight lines oriented W–E and spaced approximately 2.5 km. Several tie lines were oriented in the NW–SE and NE–SW directions. This aeromagnetic survey completely covers the studied area. The data were available in the form of magnetic anomaly contour maps at the 1 : 200,000 scale, with flight lines overlaid (Domzalski 1969). The data were digitized at the crossings of the contour lines (5 nT contour interval) with the flight lines.

The IGRF model was then extracted and substituted by a more recent model, and the corrected data were reduced to pole (RTP) (Baranov 1957). The result is presented in Fig. 4. The RTP aeromagnetic map was subjected to intensive analysis to detect the subsurface tectonic structures that affect the study area and correlate them with the results obtained from the seismic analysis. Since the metamorphic and igneous rocks that constitute the Palaeozoic basement usually have a stronger magnetic signature than Mesozoic and Cenozoic sediments, we also expected to detect with the magnetic interpretation some structures affecting the basement, which could not be imaged with the seismic reflection profiles.

Several magnetic interpretation techniques were carried out, which are explained in the next sections. First, to provide auxiliary information in the interpretation of the seismic reflection profiles, such as the existence of deep rooted fault zones, igneous structures, etc. Secondly, through 2.5-D modelling with constrains from seismic, well and outcrop data, to provide a regional setting for the

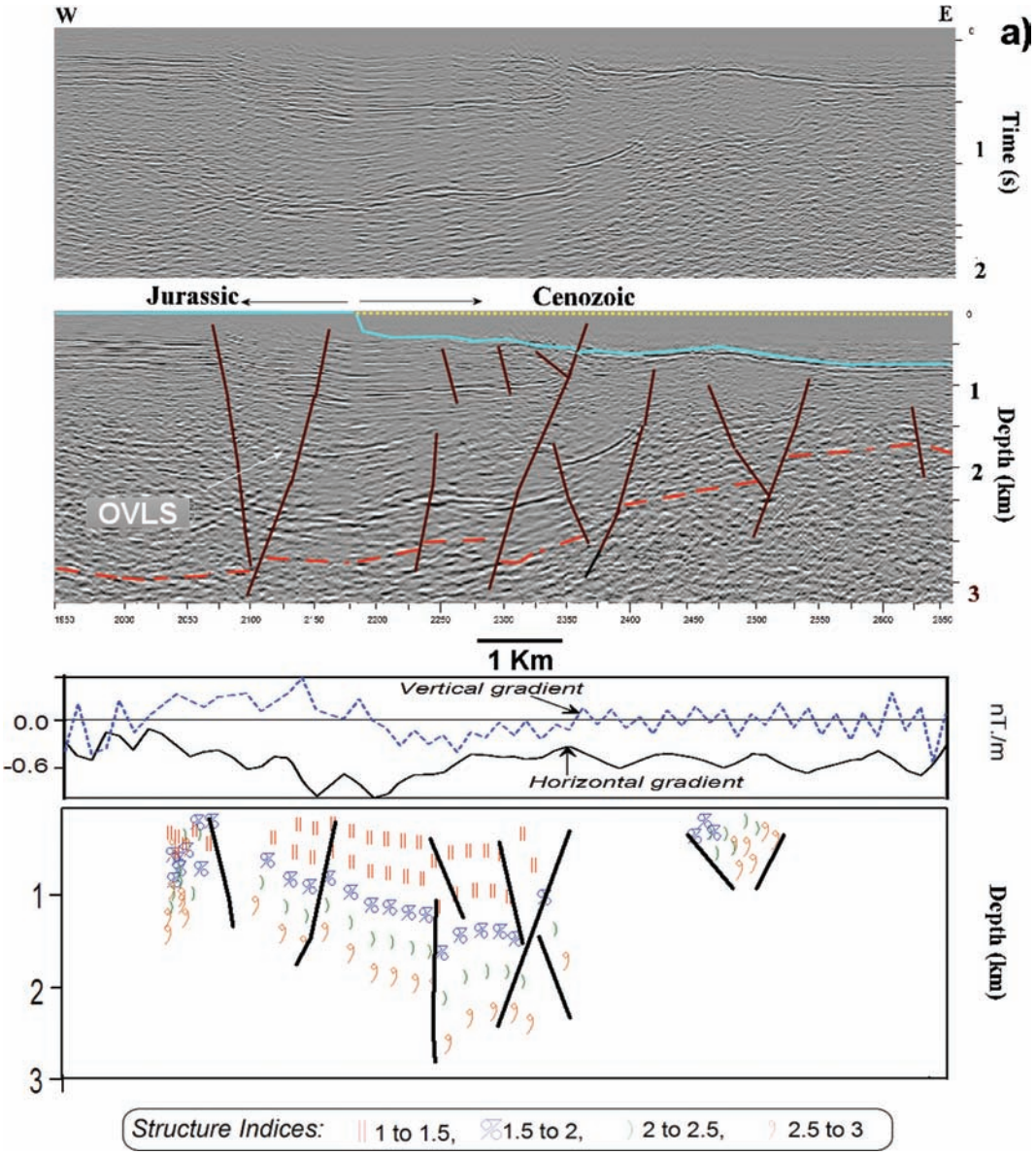

Figure 3. Sections of seismic reflection profiles shown in two-way-time (top), interpreted depth converted sections (centre) and respective magnetic interpretation (bottom), showing different aspects of the OVLS fault zone. See Fig. 2 for location. In seismic and magnetic interpretations black continuous lines indicate geological faults. The seismic interpretation is the preferred and final model: Blue line – top of Jurassic; Green line – top of Lower Cretaceous. Red dashed line- top of Palaeozoic. (c): A – NNW–SSE fault zone (see text); BF – Benavente Fault zone (see text). Magnetic interpretations presented are horizontal and vertical gradients (upper panel of bottom figure) and 2D Euler deconvolution (lower panel). Structure indices from Euler deconvolution are presented in km. Time seismic sections of parts (a) and (b) are courtesy of Mohave Oil. Part (e) is a courtesy of Deco Geophysical.

study area, in particular where no reflection data are available. Finally, by the computation of gradient, analytical signal and Euler deconvolution maps and sections, to infer the total extension of the fault zone, particularly at depth.

4.1 Construction of a structural map

Potential field data are important to delineate the tectonic fault trends using, for example, the theory of Grant & West (1965) and Linsser (1967) technique. The first horizontal gradient method was applied to the RTP aeromagnetic map. The peaks of the gradient curves were plotted and connected together to show the possible structural lines, and a structure map was obtained through this process (not shown here).

From a close examination of this structural map, it can be inferred that the OVLS fault zone has a large regional extent, extending from the southern to the northern part of the studied area. It trends approximately N–S at the southern part and changes to a NNE–SSW direction in the north. This is in agreement with the results obtained from the seismic reflection interpretation.

4.2 2.5-D modelling and analytical signal methods

The magnetic potential at a point with coordinates (x, y, z) due to an arbitrary volume of magnetic material can be expressed as (Talwani & Ewing 1960):

$$g_z = G\Delta\rho \int_{z_1}^{z_2} \int_{g_1(z)}^{g_2(z)} \frac{z_0}{x_0^2 + z_0^2} \mathrm{d}x_0 \mathrm{d}z_0 = \int_c \tan^{-1}\left(\frac{x_0}{z_{0'}}\right) \mathrm{d}z_0 \qquad (1)$$

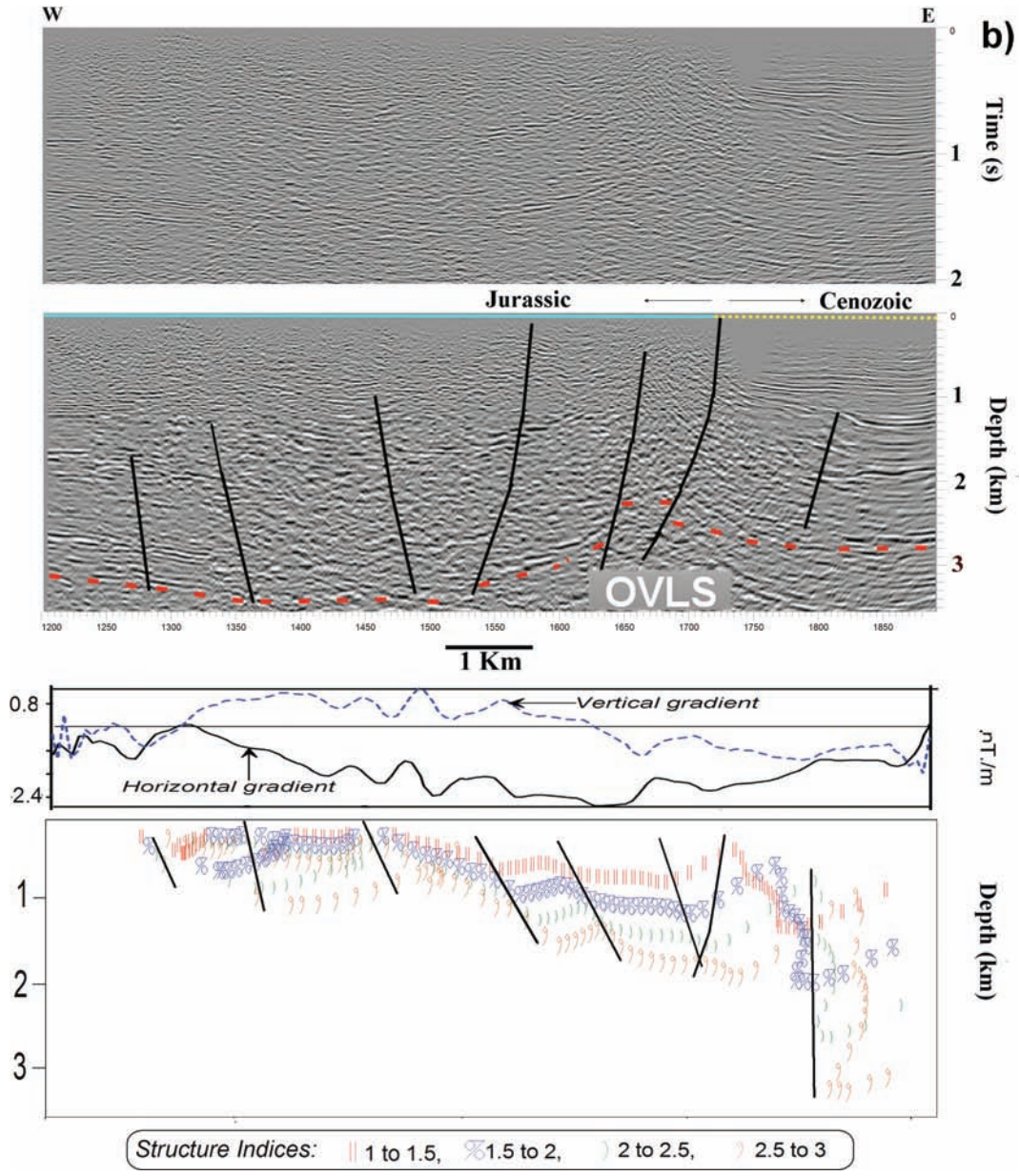

Figure 3. (*Continued.*)

where $\Delta\rho$ is a constant, G the magnetization vector and (x_o, y_o, z_o) are the coordinates of any point within the potential body. Computations of the magnetic effects by models with complex geometry were carried out using commercial software (GM-SYS 1995). 2.5-D magnetic modelling was applied to a set of four profiles perpendicular to the strike of the magnetic anomalies and covering the surveyed area (see location in Fig. 4). The purpose of these long profiles is to provide a regional setting for the different sectors of the OVLS fault zone.

The main objective was the geometry of the top of the basement and the presence of igneous structures or salt bodies, all interpreted as major contrasts in magnetization. In the area, the basement is formed by Palaeozoic igneous and metamorphic rocks. The results were checked with the analytical signal technique (Nabighian 1972) along a set of profiles. The latter method is often used to detect magnetic sources locations independent of ambient earth magnetic parameters and is currently applied for the above purposes (e.g. Roest *et al.* 1992; Wen-Bin *et al.* 2007). The depth to basement and location of igneous and salt bodies (but not faults, since these are our main target) were also analysed in all models from outcrop geological information, seismic reflection and well data, where available.

From the observation of the 2.5-D model profiles (Figs 5a–d), it can be noted that the depth to the basement rocks varies significantly. The mean depth ranges between 0.3 and 3.3 km, and a sharp discontinuity that we can associate with OVLS, is found along the profiles. This discontinuity extends from north to south, crossing the various profiles and emphasizing its regional extent. The vertical offset and its importance as a Mesozoic basin boundary structure are clear in profile 2 (Fig. 5b). In the southern profiles (profiles 3 and 4, Figs 5c and d), it no longer presents growth fault characteristics, showing a distinct Mesozoic and Cenozoic behaviour. Other major geological faults which are known to affect the basement, show up in the magnetic models such as the Nazaré fault (profile 2)

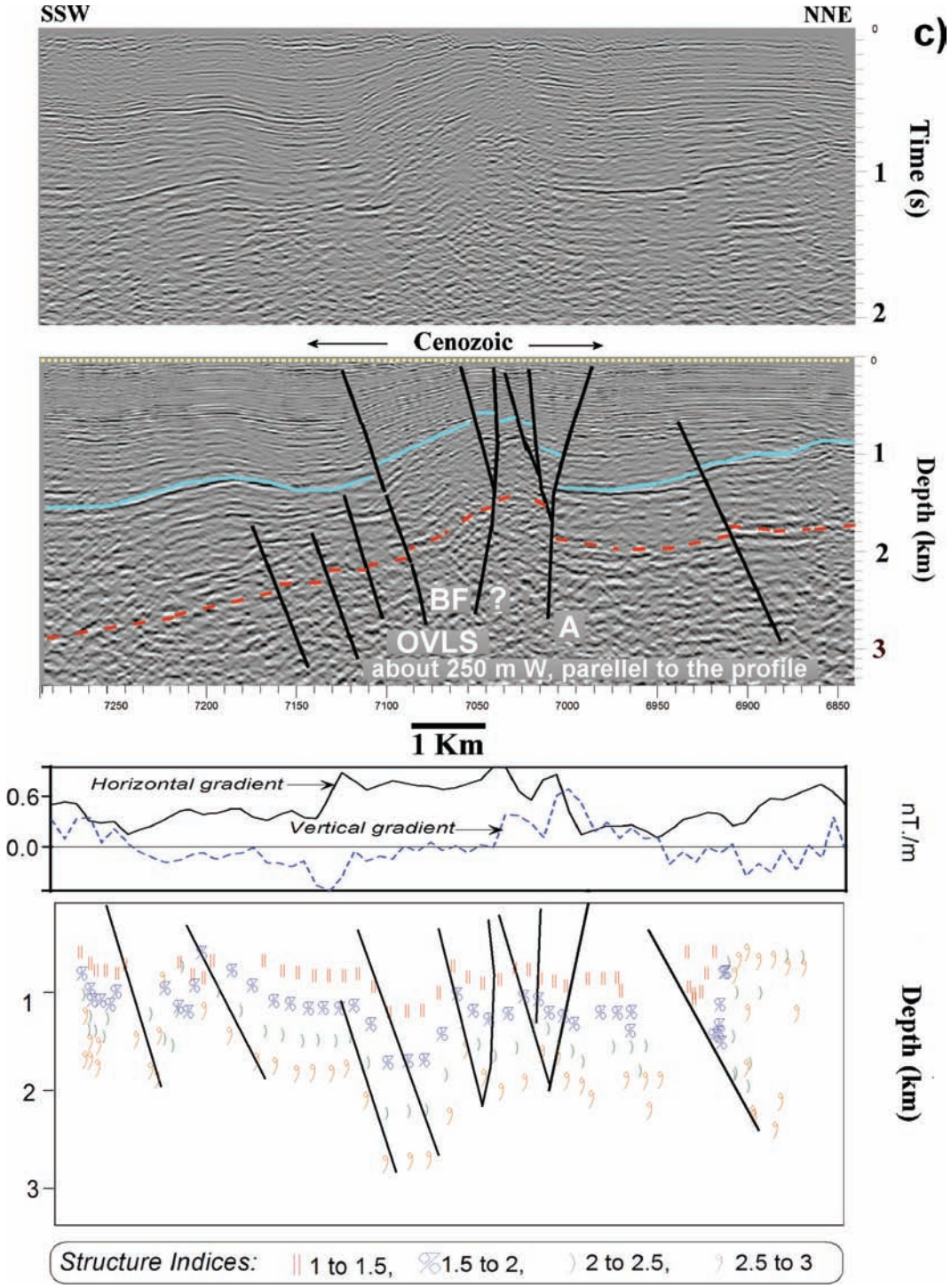

Figure 3. (*Continued.*)

and the Pinhal Novo fault (profiles 3 and 4). The magnetic susceptibilities used in the direct magnetic modelling have been listed in Table 3.

4.3 Euler deconvolution method

The Euler deconvolution method, published by Reid *et al.* (1990) tries to determine source positions and depths of the magnetic contrasts. Thompson (1982) showed that the relation of Euler's homogeneity can be written in the form

$$(x - x_0)\partial \mathbf{T}/\partial x - (y - y_0)\partial \mathbf{T}/\partial y + (z - z_0)\partial \mathbf{T}/\partial z = N(\mathbf{B} - \mathbf{T}), \quad (2)$$

where (x_0, y_0, z_0) is the position of the magnetic source whose total field **T** is detected at (x, y, z). The total field has a regional value of **B**. The degree of homogeneity N may be interpreted as a structural index (SI), which is a measure of the rate of change of the field with distance. For the index of sloping magnetic contact, the appropriate

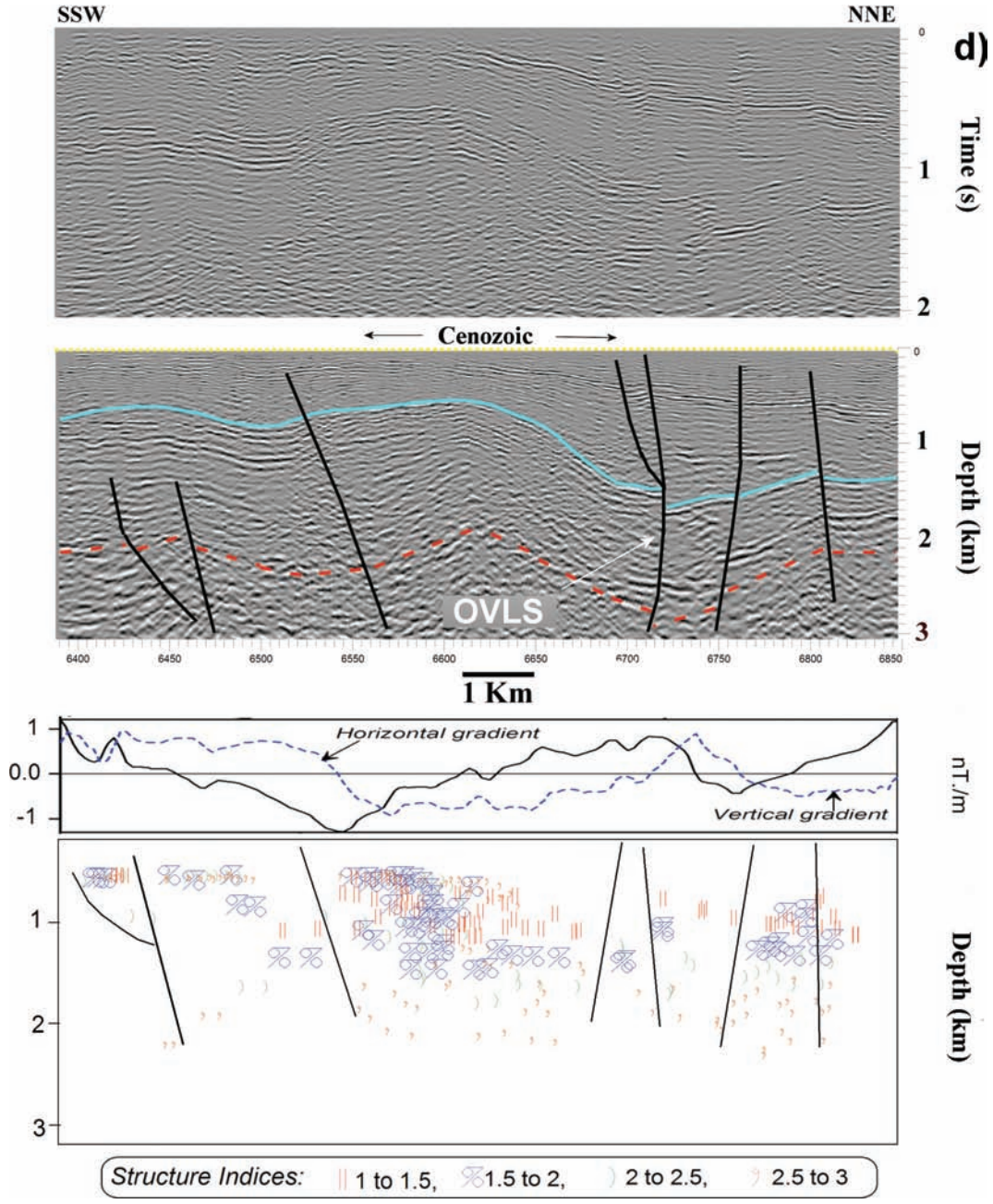

Figure 3. (*Continued.*)

form of Euler's equation is

$$(x - x_0)\partial\mathbf{T}/\partial x - (y - y_0)\partial\mathbf{T}/\partial y + (z - z_0)\partial\mathbf{T}/\partial z = A, \qquad (3)$$

where A incorporates amplitude, strike, and dip factors which cannot be separated easily.

This technique, which is applied to gridded data, measures the gradients, locates square windows of magnetic field and gradient values and determines structural windows. The results are plotted in map view (x, y), using a symbol related to depth z. The Euler deconvolution method has been applied using 0.5 magnetic step indeces to indicate the depth to the basement rocks and their structures.

The results are shown in a 2-D map, where faults inferred from seismic data are also overlaid (Fig. 6a), and in a 3-D perspective (Fig. 6b). The 3D Euler deconvolution shows that the OVLS extends from relatively shallow (200–300 m) to deep (5–6 km) depths in agreement with the seismic reflection data interpretation. The SI 2-D map indicates once more the regional extension of the OVLS fault zone. It extends from the north to the south of the studied area, varying from a NNE–SSW direction north of Lisbon to an approximate N–S direction to the south of the city. These results agree with the structure deduced from the trend analysis of aeromagnetic data and seismic reflection interpretations.

4.4 Correlation of magnetic and seismic interpretations

The 2D Euler deconvolution, gradient and analytical signal interpretation techniques were applied to magnetic profiles coincident the seismic reflection lines. The faults were derived using the 2-D Euler

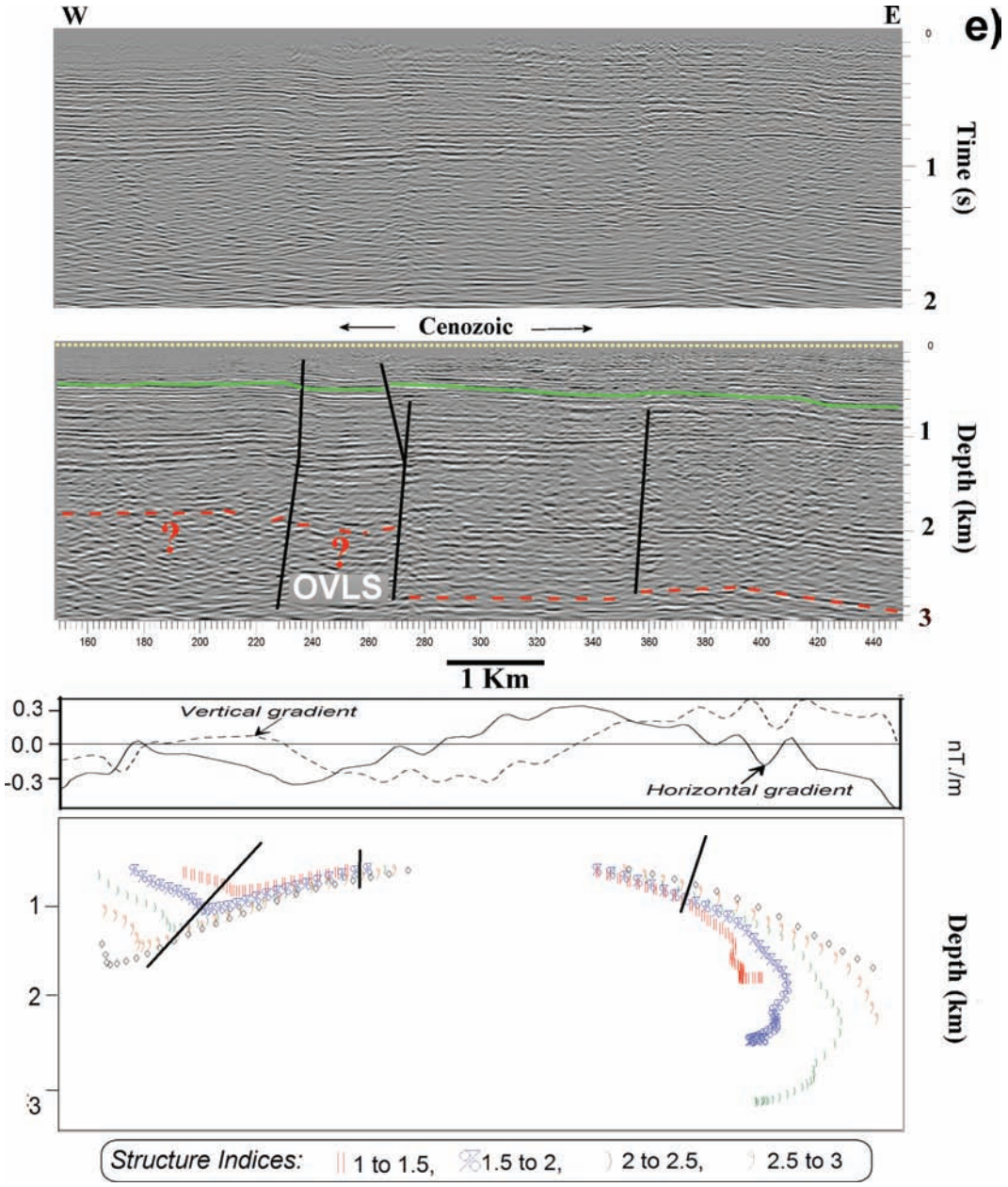

Figure 3. (*Continued.*)

deconvolution and the horizontal gradient. The results are presented in Figs 3(a)–(e), below the correspondent time and depth seismic sections. Generally, there is a good agreement between the seismic and magnetic interpretations.

Some differences found between the two interpretations arise from the fact that the two methods respond to different rock properties, and the seismic method is more suitable to image structures in the sedimentary cover, whereas the magnetic method is most appropriate to detect structures affecting the metamorphic and igneous Palaeozoic basement. Since the seismic data provides an increased resolution when compared with the magnetic data, we favour the seismic interpretation. However, the aeromagnetic data were very helpful since they confirmed the seismic interpretation in areas where the seismic signal-to-noise ratio was poor, including when the basement was shallow, and in areas where no seismic data was available. The OVLS fault zone, resulting from the integrated interpretation of geological, aeromagnetic and seismic reflection data is presented in Fig. 7 in a perspective view with the location of the full seismic reflection profiles, whose details are shown in Fig. 3.

5 SEISMICITY DATA

Relocated epicentres from the period 1970–2000 (Carrilho *et al.* 2004), where the average error (90 per cent confidence level) in the epicentral location is 5 km, were used to help to locate the major active tectonic structures and eventually the OVLS fault zone in the study area (Fig. 8). Epicentres were relocated with the software Hypocent (Lienert *et al.* 1986; Lienert & Havskov 1995), which implements a Geiger iteration scheme, with a centred, scaled and adaptively damped least-squares technique, to find the solution. The 1-D velocity model is the one routinely used for locating hypocenters

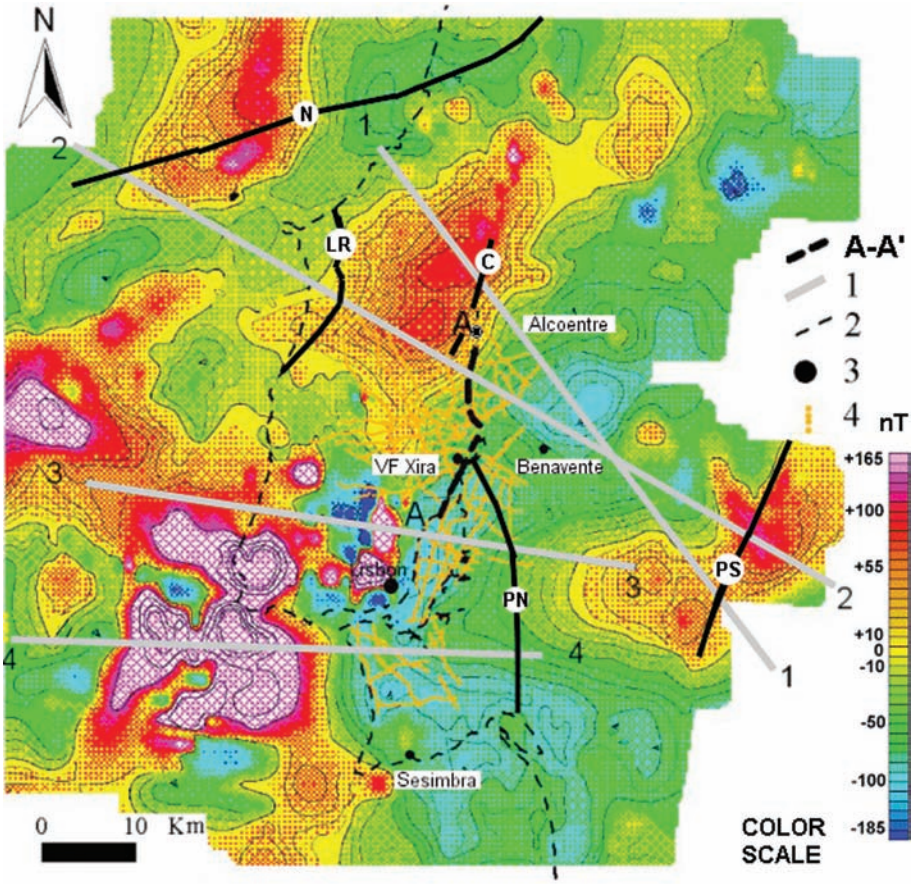

Figure 4. Aeromagnetic survey of the study area, showing the location of the regional profiles presented with 2.5-D modelling. A-A′ V. F. de Xira and Pragança sectors of the OVLS fault zone, after the seismic reflection profiles interpretation and geological outcrop studies; 1 – 2.5-D magnetic models; 2 – coastline; 3 – localities mentioned in the text; 4 – oil industry seismic-reflection profiles used for structural mapping of the basin. PN – Pinhal Novo fault; C – Cercal fault; LR – Lourinhã fault; N – Nazaré fault; PS – southern prolonging of Ponte de Soure fault (satellite lineament, Cabral & Ribeiro 1988).

in Portugal mainland, which is based in deep refraction data (e.g. Mueller *et al.* 1973; Mendes-Victor *et al.* 1980; Moreira *et al.* 1980).

The OVLS fault zone setting proposed in this paper, inferred from seismic reflection and aeromagnetic data interpretation, is shown in Fig. 8(a), together with the epicentre locations plotted with horizontal error ellipses (major error axis less than 8 km). This figure also shows the location of the cross-section (A-A′) shown in Fig. 8(b) representing the OVLS fault zone central sector (SC, Fig. 8a). In Fig. 8(a), the OVLS fault zone seems to control the distribution of the seismicity in the studied area. We can observe that the vast majority of the events are located astride or to the west of the proposed fault zone location. Epicentral locations using other seismic catalogues (e.g. ISC, On-line Bulletin, http://www.isc.ac.uk/Bull, Internat. Seis. Cent., Thatcham, United Kingdom 2001) also support this conclusion.

With the exception of five events located in the Tagus estuary, the seismicity observed further east in Fig. 8 is associated with other structures, located outside the study area. Of the five events in the Tagus estuary, the northernmost is probably associated with a NW–SE oriented fault system, detected by seismic reflection (Cabral *et al.* 2003; Carvalho *et al.* 2006; red lines, Fig. 6). The other four events can hardly be associated with any other known structure, though the Pinhal Novo fault may be a potential candidate. However, the SI map (Fig. 6) has several solutions in the same area suggesting other possible seismic sources.

Other Catalogues (Martins & Mendes-Victor 1990; Sousa *et al.* 1992), which contain events from the period 63 AD until 1992, show a similar distribution of seismicity (not shown here), with most of the earthquakes located westwards of the surface trace of the OVLS fault zone. The earthquake data catalogue used in this study, though covering a short period of time, has the advantage of possessing the information on epicentre location errors and parameters, which allows a good control of the quality of the solutions.

Hypocentre solutions have a larger error than epicentral solutions and do not allow yet a reliable analysis of the deep fault plane geometry from earthquakes hypocentre location. However a tentative correlation was tried. In Fig. 8(b), earthquakes located in a corridor containing the central sector of the OVLS (area between straight lines in Fig. 8a, SC) are plotted over a cross-section of the same sector of the fault zone. The obtained result supports the above referred distribution of the seismicity, which is in fact associated with the downwards projection of the OVLS fault zone or located to the west.

6 DISCUSSION

The studied seismic reflection data show that the OVLS fault zone, partially expressed at the surface as faults affecting Mesozoic and Cenozoic sediments or as a monocline in Cenozoic rocks, extends

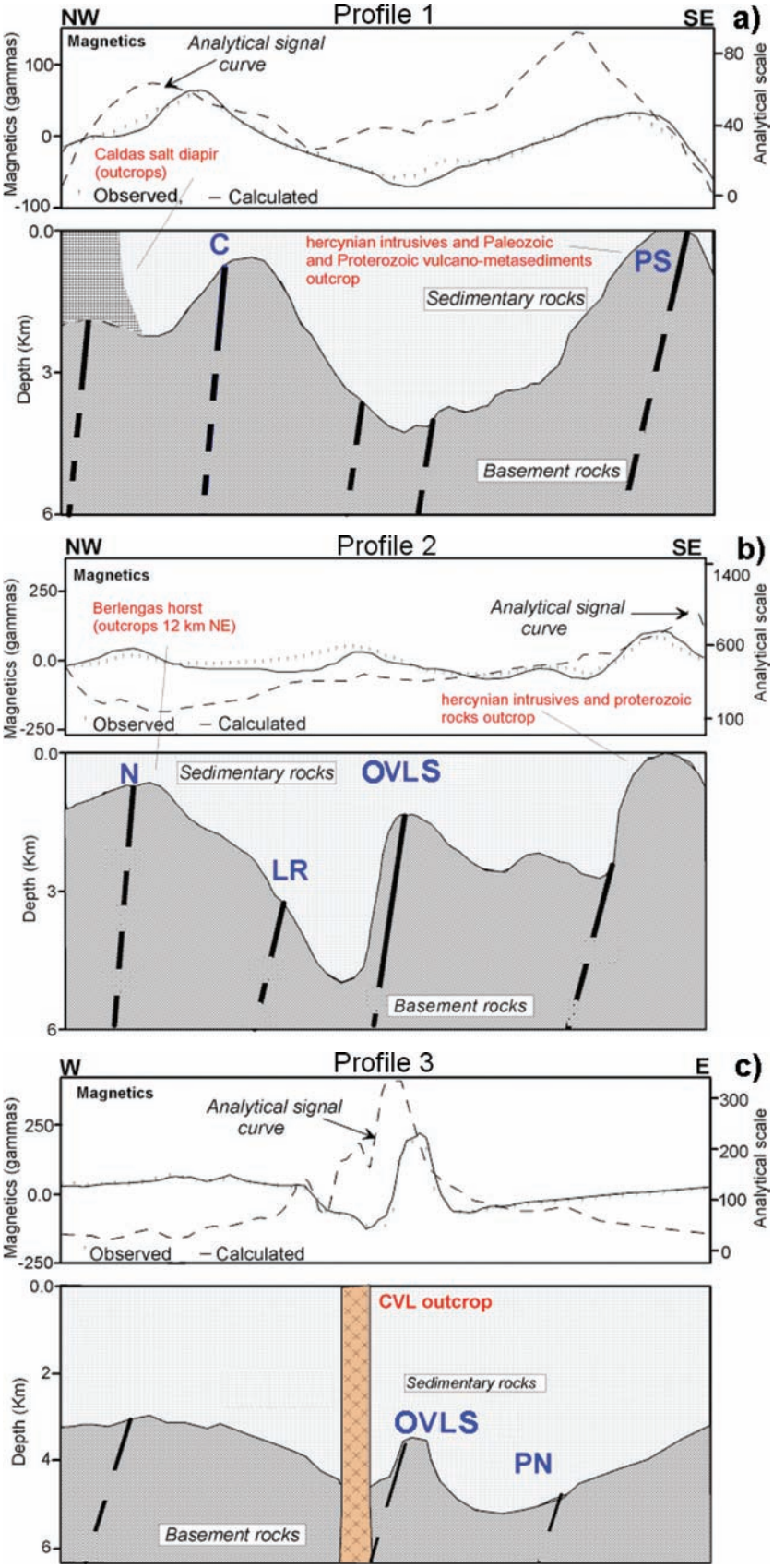

Figure 5. Schematic models of the regional magnetic profiles. PS – southern projection of Ponte de Soure fault (satellite lineament, Cabral & Ribeiro 1988); C – Cercal fault; N – Nazaré fault; LR – Lourinhã fault; PN – Pinhal Novo fault; OVLS – Ota–V. F. Xira–Lisbon–Sesimbra fault zone; CVL – Vulcanic Complex of Lisbon. For fault locations in map view please see Fig. 4.

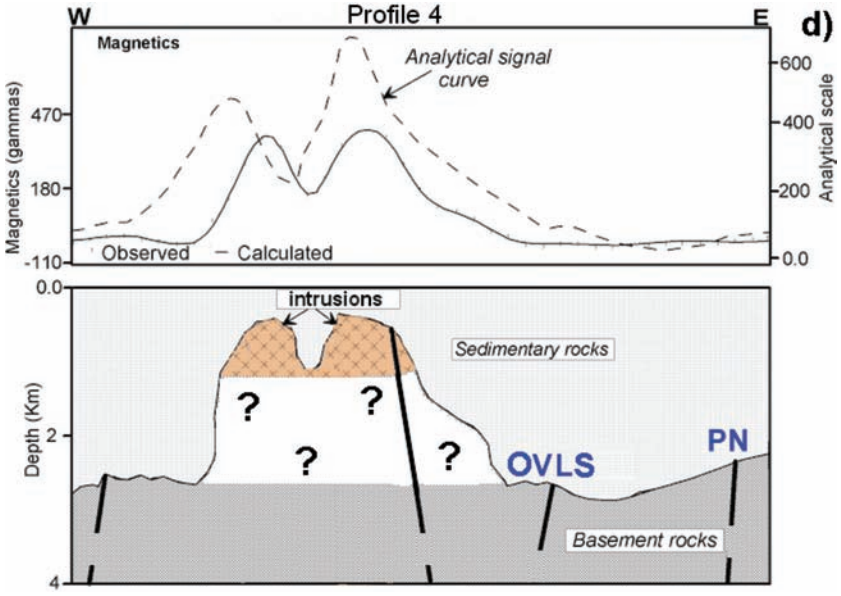

Figure 5. (*Continued.*)

Table 3. Magnetic susceptibility values used for the basement in the 2.5-D modelling of the aeromagnetic profiles shown in Fig. 5.

			End values of magnetic susceptibility	
Profile no.	Orientation	Mean magnetic susceptibility in SI units	Minimum	Maximum
Profile 1	NNW–SSE	0.0086	0.01	0.0072
Profile 2	NW–SE	0.0084	0.0098	0.007
Profile 3	W–E	0.021	0.035	0.0089
Profile 4	W–E	0.019	0.030	0.0085

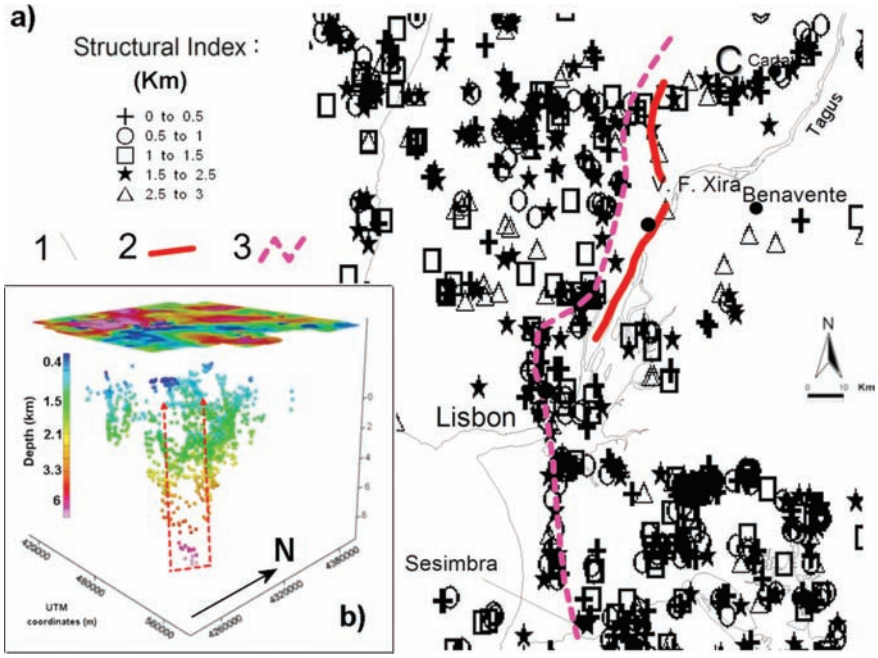

Figure 6. (a) Structural index of the RTP aeromagnetic anomaly map, obtained from Euler deconvolution. 1- coastline and river Tagus; 2- location of the Ota and Vila Franca de Xira faults in the Neogene, obtained from seismic reflection data (after Carvalho *et al.* 2006); 3- proposed location of the OVLS fault zone in the basement after seismic and magnetic data interpretation. (b) 3-D euler deconvolution of the same area showing the near surface aspect of the fault and its deep rooting.

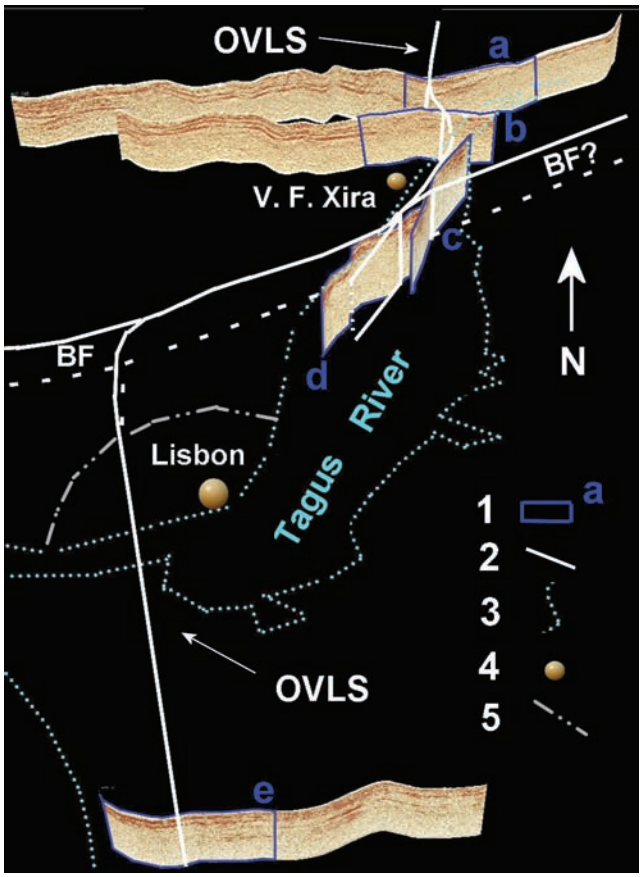

Figure 7. Perspective view of the OVLS and BF fault zones shown together with the seismic reflection profiles, after the integrated interpretation of seismic, aeromagnetic, well and geological outcrop data. 1 – Details of the seismic profiles shown in Fig. 3; 2 – fault planes; 3 – coastline; 4 – localities; 5 – Limits of the council of Lisbon. Courtesy of dGB Earth Sciences.

roughly from the latitude of Alcoentre (see Fig. 2 for location) till about 15 km north of Lisbon, consisting of two fault segments, usually referred to as the Ota (or Pragança) fault at the north and the Vila Franca de Xira fault at the south, which controlled the development of the Arruda half-graben of the LB in the Mesozoic and were strongly inverted during the Cenozoic compressive stress regime.

According to aeromagnetic data, at that location (site B, Fig. 8a), the fault zone bends westwards, outside the coverage of the available seismic reflection data, and then continues southwards with a N–S strike. Seismicity data (Fig. 8) also suggest this bend of the fault zone, since most of the earthquake locations move accordingly to the west. Unfortunately, there is not seismic reflection data available in the Lisbon area, and we cannot follow the westward bend of the fault zone.

At location B, the OVLS fault zone characteristics in the seismic reflection profiles also change (compare Figs 3a and b with Fig. 3d). In spite of the inadequate orientation of sections 3c and d relative to the fault strike, from their interpretation, it can be inferred that the vertical offsets in Cenozoic and Mesozoic rocks clearly diminish southwards. South of seismic section 3d (Fig. 2), sited to the south of location B (Fig. 8), the fault zone is no longer recognizable in the available seismic profiles, also supporting that it probably is segmented at that location, in agreement with magnetic and seismicity data.

Keller & McClay (1995) carried out 3-D sandbox modelling of positive inversion of extensional fault systems, and one of their conclusions is that fault displacements have important variations along-strike. These characteristics are found in the OVLS fault zone. The degree of inversion found at the latitude of Vila Franca de Xira (Fig. 3b) is considerably greater than at around the latitude of Ota (Fig. 3a) and further south (Figs 3c–e).

Keller & McClay (1995) further conclude that extension and inversion produce strongly segmented faults, with fault segments dying out laterally or overlapping across displacement transfer zones in the form of relay ramp structures. Therefore, the segmentation of the OVLS fault zone is in agreement with 3-D scaled analogue models and with data from other areas, which have undergone positive inversion (e.g. Knott *et al.* 1995). The fact that a fault segment continues for a few kilometres (5–6 km) southwards of the transfer zone location B (Figs 7 and 8), is compatible with the results of Keller & McClay (1995).

As stated above, according to the magnetic and seismicity data, the OVLS fault zone jumps westwards at location B, through a right lateral stepover about 9–10 km wide (outside the coverage of the seismic reflection data). Then it strikes N–S towards Lisbon, crossing the city area at depth, and enters the Setúbal Península (Figs 7 and 8), where seismic reflection data are also available, being detected until near the village of Sesimbra, at the south (Fig. 1). The seismic reflection data in the Setúbal Peninsula show that the fault zone cuts the Palaeozoic, Mesozoic and Cenozoic geological units, although producing relatively small vertical offsets in the Cenozoic (Fig. 3e). The small deformation of the Cenozoic horizons contrasts with the much larger deformation evidenced in the seismic profiles located to the north of Lisbon, where the inversion of the extensional Mesozoic structures is large. This indicates that this southern segment of the OVFXS fault zone in the Palaeozoic basement was subjected to small dip-slip reactivation in the Cenozoic compressive tectonic regime, strongly contrasting with the behaviour of the northern Vila Franca de Xira and Ota segments.

The bend or segmentation of the OVLS fault zone at location B approximately coincides with the eastern sector of a probable ENE–WSW trending, north verging reverse fault at depth, which controls the elongated Sintra–Caneças antiformal structure located to the west, bordering the northern limit of the Sintra massif (Cabral 2008). This suggests interference between the two structures, with the OVLS fault zone probably offset by the WSW–ENE fault.

Some evidence of the eastwards prolonging of the WSW–ENE fault zone under the Holocene sediments of the Tagus river alluvial plain comes from the seismic reflection data (seismic profiles S1, 229, 223, S6 and 240, from the Samora and Barreiro surveys described in Table 1). The profile in Fig. 3(c) also shows two faults compatible with this structure. The northernmost (signalled A in the figure) probably corresponds to an approximate NW–SE trending fault of the above referred Porto Alto fault system (Carvalho *et al.* 2006). The other fault with down throw to the NNE (signaled BF in Fig. 3c) may be connected with the WSW–ENE fault zone under discussion. The interpretation of the profiles available in the area is thus compatible with a structure with the expected location and geometry, though the detectable vertical offset of this fault is only of several tens of metres in the Cenozoic layers. Fig. 8 also shows that a few earthquakes can be associated with this fault.

Stich *et al.* (2005) have recently calculated a moment tensor solution of the 1909 Benavente earthquake, evidencing a dip-slip reverse component with nodal planes presenting strike/dip/rake of N51°E/52°/83° and N242°E/38°/99°. Therefore, the proposed eastern prolonging of the WSW–ENE fault zone presented here is a

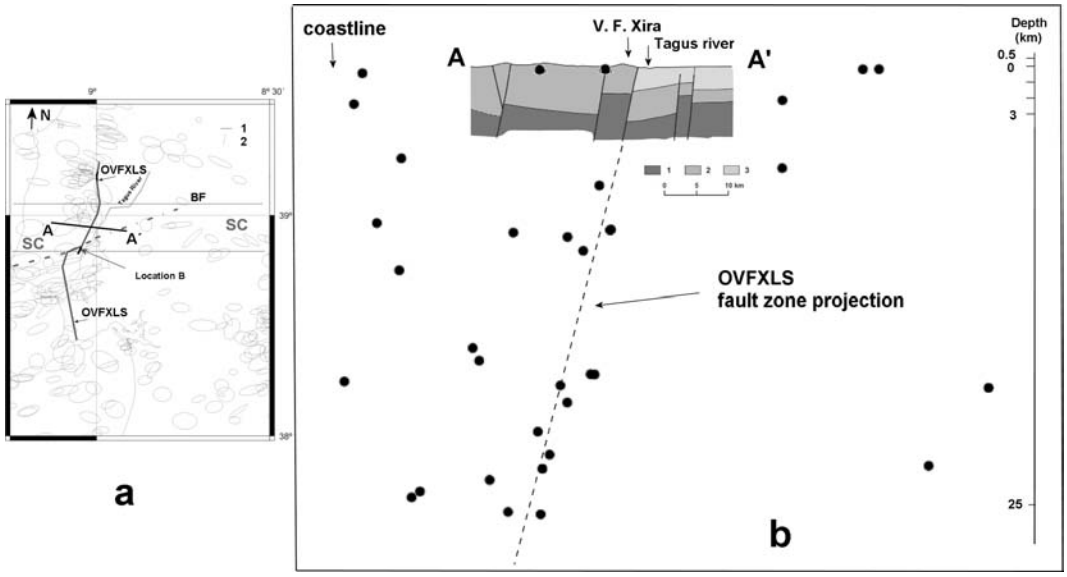

Figure 8. (a) Seismicity in the study region and adjacent areas for the period 1970–2000 (after Carrilho *et al.* 2004), plotted with error ellipses of epicentre location. All events have a major axis of error less than 8 km. Also shown are the locations of the OVLS fault zone and the Benavente fault (BF) proposed in this work (dash and dash-dot, west and east of the Tagus river, respectively). 1- coastline; 2- delimitation of the different sectors of the OVLS fault zone. SC- central sector of the OVLS fault zone. A-A′ – cross-section presented in part (b). (b) Geological cross-section obtained by an integrated interpretation of magnetic, seismic, well and geological outcrop data, with relocated epicentres of the central sector of the fault zone (location in a). Note the association of the projected fault plane and several events. 1 – Palaeozoic basement; 2 – Mesozoic; 3 – Cenozoic.

possible candidate for the location of the 1909 Benavente earthquake, as it trends approximately parallel to the first aforementioned nodal plane. We hereinafter refer to this structure as the Benavente fault zone.

The models of the magnetic profiles shown in Fig. 5 confirm the interpretation of the seismic reflection profiles and show with simplicity several aspects of the regional structure of the study area. The model of profile 2 shows that the border of the Mesozoic LB in this area is represented by the northern segment of the OVLS fault zone (see Fig. 4 for location). Since magnetic data respond mainly to variations in the basement (Palaeozoic igneous and metamorphic rocks) properties and structure, we have not marked any faults in the Mesozoic and Cenozoic units, though the examples of Fig. 3 show that the magnetic method is also able to detect major faults in the sedimentary column, probably due to the large volumes of sedimentary material. However, from the seismic data (Figs 3a and b), we can see that the fault was reactivated in the Cenozoic, with splay faults probably nucleating from the tip of the previous normal fault and propagating towards the east, as suggested from analogue scaled models (Eisenstadt & Withjack 1995; McClay 1995; Eisenstadt & Sims 2005).

Profile 1, also crossing the northern sector of the OVLS fault zone, shows that the thickness of the Mesozoic sediments diminishes to the north, with the LB's major boundary fault corresponding here to the Cercal (or Montejunto) fault (Carvalho *et al.* 2005). On the contrary, the LTCB shows an increased thickness, though part of the modelled anomaly source maybe caused by lithological variations inside the basement, as a maximum thickness of 4 km of sediments at this location is not credible.

A few kilometres southward of the OVLS fault segmentation at location B, profile 3 (Fig. 5c) shows that the fault zone looses expression, evidencing a much smaller vertical offset. Further south, in the Setúbal Peninsula, profile 4 (Fig. 5d) evidences that the southern segment the OVXLS fault zone produces a much reduced vertical offset in the Palaeozoic basement although seismic data suggests (Fig. 3e) a larger vertical offset. Though this fault may probably have been a pre-inversion fault, seismic (no growth is observed in Jurassic sediments) and aeromagnetic data show that it was not the Mesozoic Basin boundary fault zone, as the fault segments to the north of location B were.

Reactivation of previous weakness zones is a common situation. At location B, the OVLS fault zone is apparently right-laterally offset across the proposed Benavente fault, and southwards it changes to an N–S strike (Fig. 7), which is a less favourable orientation for reactivation with positive inversion under the Cenozoic compressive stress regime. The fault becomes more high-angle, which also makes it less favourable for a positive inversion reactivation (Lowell 1995).

Under a change in the stress regime, normal faults with listric geometry striking perpendicular to a horizontal maximum compressive stress should be reactivated with a predominant reverse movement component (Lowell 1995; Sibson 1995). Steep faults with a reduced angle to that maximum compressive stress are commonly reactivated with a predominant strike-slip movement component (Lowell 1995). When the angle of pre-existing faults with the direction of the maximum compressive is relatively high, transpression is the most common mode of inversion (Lowell 1995).

Furthermore, when the strike-slip component is dominant, relatively high-angle normal faults can be reactivated and no new structures need to be created. When reverse kinematics dominates, some of the older faults may be reactivated, and new reverse structures are formed. The geometries inherited from the previous extensional episode are of great importance to the positive inversion structures (Yamada & McClay 2003). These empirical observations, found throughout the world, seem to be in agreement with the behaviour of the OVLS and Benavente fault zones.

The northern and central segments of the fault (from location B to approximately the town of Ota) trend NNE–SSW to N–S, at a high-angle to the dominant Cenozoic compressive stress, which trended NW–SE (Ribeiro *et al.* 1990). Here, clear reverse structures

affecting Cenozoic sediments can be observed (Figs 3a and b), indicating that, as expected, the reverse component predominates. As referred above, in this sector some of the Mesozoic basin boundary faults have been inverted, namely the Vila Franca de Xira and Ota (or Pragança fault). A variable degree of inversion is found for several previously normal faults that present the same strike. A selective reactivation of previous normal faults is common in positive inversion situations (e.g. Lowell 1995; Sibson 1995).

The N–S oriented southern segment of the fault trends at an angle of approximately 45° to the usually admitted strike of the compressive stress in the Cenozoic (Ribeiro *et al.* 1990, 1996). This has been considered the limit between a predominantly reverse inversion and dominant strike-slip reactivation (Lowell 1995). Therefore, in this segment of the fault zone, it is expected the reactivation of preexisting normal faults with mostly strike-slip movement component and without the development of new reverse structures, corresponding to incipient inversion. This is what we observe on the seismic reflection sections of the Setúbal Península (see Fig. 3e), which bear no seismic signature of important reverse structures in the Cenozoic sedimentary cover.

Finally, some considerations should be made about the possibility that the OVLS fault zone is an active seismogenic source and, if so, of its implication on seismic potential assessment. The present tectonic activity of the OVLS fault zone implies the reactivation of this structure under the present stress regime, which is oriented approximately NW–SE to WNW–ESE in the study area (Ribeiro *et al.* 1996; Borges *et al.* 2001). As stated before, the fault zone seems to control the distribution of the seismicity in the study area (Fig. 8a). The geological cross-section presented in Fig. 8(b), located in the central sector of the OVLS fault zone and with epicentres from this sector overlaid, results from the integrated interpretation of seismic reflection, aeromagnetic, well and geological outcrop data. The downward projection of the OVLS confirms that the epicenters distribution is indeed connected to the westwards dip of the fault surface and with other structures located to the west (Fig. 8b).

Other evidences suggest that the OVLS fault zone is very probably active. From outcrop geological studies, the fault is known to affect upper Miocene sediments and it is parallel to other structures in the LTCB, which also affect sediments of this age and are known to be active in the Pleistocene, as the Azambuja fault (Cabral *et al.* 2003, 2004). Moreover, geophysical data recently acquired near Vila Franca de Xira and well data (Carvalho *et al.* 2006) suggest that in this segment, the fault cuts Quaternary sediments and a vertical offset of 5m was estimated.

7 CONCLUSIONS

The aim of this work was to investigate a regional fault zone that is known to exist in the LTV, from geological and seismic reflection data. This structure has been previously considered as an important structure in the regional seismotectonics framework and a possible source of the significant seismicity that affects the study region.

In its northern and central sectors, it corresponds to an approximately NNE–SSW to N–S oriented, reverse fault zone that borders the LB and the LTCB, approximately from north of Ota till about 8–9 km south of Vila Franca de Xira. Reprocessed and reinterpreted seismic reflection, aeromagnetic and seismicity data presented here confirm that the fault zone extends along that distance, for about 35 km. In these sectors, the fault comprises two segments resulting from the inversion of previous normal boundary faults of the Mesozoic LB, namely the Vila Franca de Xira fault at the south and the Ota (or Pragança) fault at the north.

To the south, according to the interpreted aeromagnetic data, the OVFXS fault zone does not end about 8–9 km south of Vila Franca de Xira, as previously thought, but it bends westwards as it crosses the proposed WSW–ENE trending Benavente fault and continues south with an approximate N–S strike, under the city of Lisbon and crossing the Setúbal Peninsula until the village of Sesimbra.

This previously unknown segment of the OVLS fault zone, at least 45 km long, is supported by seismic reflection data in the Setúbal Península and is also sustained by earthquake distribution data. The former data show that the fault zone is steeper in this segment and that the deformation that it produces in the Cenozoic sediments is considerably less than in the northern segments. The difference in character of the fault from north to south is also inferred from 2.5-D magnetic modelling. Epicentre locations are mostly located to the west of the three sectors, which, associated with the continuity of Euler solutions of the aeromagnetic data, suggest that we have a single major fault zone, though segmented.

In face of this, we propose that the fault zone should be cited as the Ota–Vila Franca de Xira–Lisboa–Sesimbra (OVLS) fault zone. Interpretation of seismic and magnetic data shows that in all segments the fault extends to at least 5–6 km depth. In spite of poor hypocenter locations, an association between the downdip prolonging of the fault surface, as seen from the seismic data in the first 2–3 km, and the hypocentre solutions at depth is apparent. Moreover, this structure seems to delimit a crustal domain located to the west, characterized by a higher seismic activity.

The newly proposed WSW–ENE Benavente fault zone was deduced from the observation that the bend of the OVLS fault zone coincides with the eastern end of the Sintra–Caneças structural alignment, and that the related fault at depth apparently continues further east under the Tagus river alluvial sediments, as suggested by seismic reflection data. A moment tensor solution recently computed for the 1909 Benavente earthquake points to an almost pure reverse movement on a fault with a similar strike. Together with the fact that the proposed Benavente fault zone passes 1–2 km south of Benavente, makes it a candidate structure as the source of the 1909 earthquake. A more refined interpretation of the section of this fault under the Tagus Holocene alluvia, using seismic reflection and potential field data, needs to be carried out.

The results presented here point to the importance of local seismogenic sources in the seismic hazard estimation of the study area, in agreement with previous work of several authors (Peláez *et al.* 2002; Cabral *et al.* 2003, 2004; Vilanova & Fonseca 2004; Carvalho *et al.* 2006). Further studies, using more reprocessed seismic reflection data, topographic, satellite interferometry, gravimetric and Moho data are currently underway to provide a better understanding of the study area.

ACKNOWLEDGMENTS

Part of this work was funded by the portuguese Foundation for Science and Technology and the EC under Project Sismotecto (POCI/CTE-GIN/58250/2004). The Department of Prospecção e Exploração de Petróleos from the Direcção Geral de Geologia e Energia is greatly acknowledged for supplying the seismic reflection data, as well as Mohave Oil for allowing the publication of their prestack time migrated reprocessed data. We also thank Deco Geophysical for allowing the publication of reprocessed seismic reflection data in the Peninsula of Setúbal. Our special thanks to the Centro de Geofísica da Universidade de Lisboa for several contributions to this study. The support of the head of the Geophysics Division of the

Instituto Nacional de Engenharia, Tecnlogia e Inovação to this project, Luís Martins is also acknowledged. Our thanks to Arnaud Huck and dGB Earth Sciences for allowing the publication of Fig. 7. The authors would also like to thank those who contributed to the final results presented here: Ruben Dias, Luís Matias, Catarina Moniz, Luís Torres and Manuela Costa for discussions on the interpretation of the seismic reflection profiles and geodynamic implications of the results. We are also indebted to the contributions made by two anonymous reviewers, who greatly improved the original version of the manuscript.

REFERENCES

Baptista, M.A., Miranda, J.M., Chierici, F. & Zitellini, N., 2003. New study of the 1755 earthquake source based on multi-channel seismic survey data and tsunami modelling, *Nat. Hazards Earth Sys. Sci.,* **3,** 333–340.

Baranov, V., 1957. A new method for interpretation of aeromagnetic maps – pseudo gravity anomalies, *Geophysics,* **22,** 359–383.

Borges, J.F., Fitas, A.J.S., Bezzeghoud, M. & Teves-Costa, P., 2001. Seismotectonics of Portugal and its adjacent Atlantic area, *Tectonophysics,* **337,** 373–387.

Cabral, J., 2008. Tectónica, *in Notícia Explicativa da Folha 34-B (Loures),* da Carta Geológica de Portugal na Escala 1/50.000, INETI, Lisbon-Portugal, Portugal.

Cabral, J. & Ribeiro P., 1988. *Carta Neotectónica de Portugal Continental (escala 1:1000.000),* Geological Survey of Portugal, Geology Dep. Fac. Science, Cabinet of Nuclear Safety and Protection.

Cabral, J., Moniz, C., Ribeiro, P., Terrinha, P. & Matias, L., 2003. Analysis of seismic reflection data as a tool for the seismotectonic assessment of a low activity intraplate basin- the Lower Tagus Valley (Portugal), *J. Seism.,* **7,** 431–447.

Cabral, J., Ribeiro P., Figueiredo P., Pimentel N. & Martins A., 2004. The Azambuja fault: an active structure located in an intraplate basin with significant seismicity (Lower Tagus Valley, Portugal), *J. Seism.,* **8,** 347–362.

Carrilho, F., Nunes, J.C., Pena, J. & Senos, M.L., 2004. *Catálogo Sísmico de Portugal Continental e Região Adjacente para o período 1970–2000,* Instituto de Meteorologia, ISBN 972-9083-12-6.

Carvalho, J., 2003. Sísmica de alta resolução aplicada à prospecção, geotecnia e risco sísmico, *PhD thesis*. University of Lisbon.

Carvalho, J., Matias, H., Torres, L., Manupella, G., Pereira, R. & Mendes-Victor, L., 2005. The structural and sedimentary evolution of the Arruda and Lower Tagus Sub-Basins, Portugal, *Mar. Petrol. Geol.,* **22,** 427–453.

Carvalho, J., Cabral, J., Gonçalves, R., Torres, L. & Mendes-Victor, L., 2006. Geophysical methods applied to fault characterization and earthquake potential assessment in the lower Tagus valley, Portugal, *Tectonophysics,* **418,** 277–297.

Dineva, S., Batlló, J., Mihaylov, D. & van Eck, T., 2002. Source parameters of four strong earthquakes in Bulgaria and Portugal at the beginning of the 20th century. *J. Seism.,* **6,** 99–123.

Domzalski, W., 1969. Interpretation of an aeromagnetic survey offshore Portugal (1:200.000), Fairey Surveys Ltd. report.

Eisenstadt, G. & Sims, D., 2005. Evaluating sand and clay models: Do rheological differences matter? *J. Struct. Geol.,* **27,** 1399–1412.

Eisenstadt, G. & Withjack, M.O., 1995. Estimating inversion: results from clay models, in *Basin Inversion,* pp. 119–136, eds Buchanan, J.G. & Buchanan, P.G., Geological Society Special Publication, No. 18, Oxford.

GM-SYS, 1995. *Gravity and Magnetic Modelling Version 3.6, Northwest Geophysical Association,* Inc.(NGA), Oregon, USA.

GPEP, 1986. *Petroleum Potential of Portugal,* p. 62, Gabinete para a Pesquisa e Exploração de Petróleos, Lisboa.

Grant, F.S. & West, G.F., 1965. *Interpretation Theory in Applied Geophysics,* MacGraw-Hill, New York.

Gràcia, E., Dañobeitia, J., Vergés, J. & the PARSIFAL Team (N. Zitellini, M. Rovere, D. Accetella, A. Ribeiro, J. Cabral, L. Matias, R. Bartolomé, M. Farrán, D. Casas, A. Maldonado, A. Pazos, D. Córdoba and X. Roset), 2003. Mapping active faults offshore Portugal (36°N–38°N): implications for seismic hazard assessment along the southwest Iberian margin, *Geology,* **31,** 83–86.

Jaspen, P., 1993. Influence of lithology and neogene uplift on seismic velocities in Denmark: implications for depth conversion of maps, *Am. Assoc. Petrol. Geol. Bull.,* **77,** 194–211.

Justo, J.L. & Salwa, C., 1998. The 1531 Lisbon earthquake, *Bull. seism. Soc. Am.,* **88,** 319–328.

Keller, J.V.A. & McClay, K.R., 1995. 3D sandbox of positive inversion, in *Basin Inversion,* pp. 137–146, eds Buchanan, J.G. & Buchanan, P.G., Geological Society Special Publication, No. 18, Oxford.

Knott, S.D., Beach, A., Welbon, A.I. & Brockbank, P.J., 1995. Basin inversion in the gulf of Suez, in *Basin Inversion,* pp. 59–81, eds Buchanan, J.G. & Buchanan, P.G., Geological Society Special Publication, No. 18, Oxford.

Leinfelder, R.R. & Wilson, R.C.L., 1998. Third-order sequences in an Upper Jurassic Rift-related second-order sequence, central Lusitanian basin, Portugal, in *Mesozoic and Cenozoic Sequence Stratigraphy of European Basins,* pp. 507–525, eds Graciansky, P.C., Hardenbol, J., Jacquin, T. & Vail, P.R., SEPM Special Publication No. 60.

Lienert, B. & Havskov, J., 1995. A computer program for locating earthquakes both locally and globally, *Seism. Res. Lett.,* **66,** 26–36.

Lienert, B., Berg, E. & Neil Frazer, L., 1986. Hypocenter: an earthquake location method using centered, scaled and adaptively damped least squares, *Bull. seism. Soc. Am.,* **76,** 771–783.

Linsser, H., 1967. Investigation of tectonic by gravity detailing, *Geophys. Prospect.,* **15,** 480–515.

Lomholt, S., Rasmussen, E.S., Andersen, C., Vejbaek, O.V., Madsen, L. & Steinhardt, H., 1995. Seismic interpretation and mapping of the Lusitanian Basin, Portugal, p. 70, *Final Report, Proj. MILUPOBAS, Contract No. JOU-CT94-0348, GEUS*, Copenhagen.

Lowell, J.D., 1995. Mechanics of basin inversion from world wide examples, in *Basin Inversion,* pp. 39–57, eds Buchanan, J.G. & Buchanan, P.G., Geological Society Special Publication, No. 18, Oxford.

Marsden, D., 1989. Layer cake depth conversion, *Leading Edge,* **1,** 10–14.

Martins, I. & Mendes-Víctor, L.A., 1990. *Contribuição para o Estudo da Sismicidade de Portugal Continental,* Instituto Geofísico Infante D. Luís, Publicação 18, University of Lisbon, Lisboa.

McClay, K.R., 1995. The geometries and kinematics of inverted fault systems: a review of analogue model studies, in *Basin Inversion,* pp. 97–118, eds Buchanan, J.G. & Buchanan, P.G., Geological Society Special Publication, No. 18, Oxford.

Mendes-Victor, L.A., Hirn, A. & Veinant, J.L., 1980. A seismic section across the Tagus Valley, Portugal: possible evolution of the crust, *Ann. Geophys.,* **36,** 469–476.

Mezcua, J., 1982. *Catalogo General de Isossistas de la Peninsula Iberica,* Instituto Geografico Nacional, Publicación 202, Madrid.

Moreira, V.S., 1984. Sismicidade histórica de Portugal Continental, *Revista Instituto Nacional Meteorologia e Geofísica,* **3,** 3–79.

Moreira, V.S., 1985. Seismotectonics of Portugal and its adjacent area in the Atlantic, *Tectonophysics,* **117,** 85–96.

Moreira, V.S., Prodehl, C., Mueller, St. & Mendes, A.S., 1980. Crustal Structure of Western Portugal, in *Proc. 17Th Assembly of the ESC*, Budapest, 529–532.

Mueller, S., Prodehl, C., Mendes, A.S. & Moreira, V.S., 1973. Crustal structure in the southwestern part of the Iberian Peninsula, *Tectonophysics,* **20,** 307–318.

Nabighian M.N., 1972. The analytic signal of two-dimensional magnetic bodies with polynomial cross-sections; its properties and use for automated anomaly interpretation, *Geophysics,* **37,** 505–517.

Oliveira, C.S., 1986. *A Sismicidade Histórica e a Revisão do Catálogo Sísmico,* LNEC, Proc. 36/11/7368, I e D, Estruturas, Relatório 99/86 – NDA, Lisboa.

Oliveira, T., Ramalho, M., Antunes, M.T., Monteiro, J.H. & Carvalho, D., 1992. *Carta Geológica de Portugal, escala 1: 500.000,* Serviços Geológicos de Portugal, Lisboa

Peláez, J.A.M., Casado, C.L. & Romero, J.H. 2002. Deaggregation in magnitude, distance, and azimuth in the south and west of the Iberia Peninsula, *Bull. seism. Soc. Am.,* **92**(6), 2177–2185.

Rasmussen, Erik S., Lomholt, S., Anderson, C. & Vejbaek, O.V., 1998. Aspects of the structural evolution of the Lusitanian Basin in Portugal and the shelf and slope area offshore Portugal, *Tectonophysics,* **300,** 199–225.

Reid, A.B., Allsop, J.M., Granser, H., Millet, A.J. & Somerton, I.W., 1990. Magnetic interpretation in three dimensions using Euler deconvolution, *Geophysics,* **55,** 80–91.

Ribeiro, A., Kullberg, M.C., Kullberg, J.C., Manupella, G. & Phipps, S., 1990. A review of Alpine tectonics in Portugal: foreland detachment in basement and cover rocks, *Tectonophysics,* **184,** 357–366.

Ribeiro, A., Cabral, J., Baptista, R. & Matias, L., 1996. Stress pattern in Portugal mainland and the adjacent Atlantic region, West Ibéria, *Tectonics,* **15,** 641–659.

Roest, W.R., Verhoef, J. & Pilkington, M., 1992. Magnetic interpretation using the 3D analytical signal, *Geophysics,* **57,** 116–125.

Sibson, R.H., 1995. Selective fault reactivation during basin inversion: potential for fluid redistribution through fault-valve action, in *Basin Inversion,* pp. 3–19, eds Buchanan, J.G. & Buchanan, P.G., Geological Society Special Publication, No. 18, Oxford.

Sousa, M.L., Matins, A. & Oliveira, C.S., 1992. *Compilação de Catálogos Sísmicos da Região Ibérica,* LNEC, Relatório 36/92 – NDA, Dep. Estruturas, Núcleo Dinâmica Aplicada, Proc. 036/11/9295, Lisboa.

Stich, D., Batlló, J., Macià, R., Teves-Costa, P. & Morales, J., 2005. Moment tensor inversion with single-component historical seismograms: the 1909 Benavente (Portugal) and Lambesc (France) earthquakes, *Geophys. J. Int.,* **162,** 850–858.

Talwani, M. & Ewing, M., 1960. Rapid computation of gravitational attraction of three-dimensional bodies of arbitrary shape, *Geophysics,* **25,** 203–225.

Teves-Costa, P., Rio, I., Marreiros, C., Ribeiro, R. & Borges, J.F., 1999. Source parameters of old earthquakes: semi-automatic digitalization of analog records and seismic moment assessment, *Nat. Hazards,* **19,** 205–220.

Thompson, D.T., 1982. EULDPH – a new technique for making computer-assisted depth estimates from magnetic data, *Geophysics,* **47,** 31–37.

Vilanova, S.P. & Fonseca, J.F.B.D., 2004. Seismic hazard impact of the Lower Tagus Valley Fault Zone (SW Iberia), *J. Seism.,* **8,** 331–345.

Vilanova, S.P., Nunes, C.F. & Fonseca, J.F.B.D., 2003. Lisbon 1755: a case of triggered onshore rupture? *Bull. seismol. Soc. Am.,* **93,** 2056–2068.

Walker, D.J., 1983. *Final Report: Seismic Interpretation, Lusitanian basin, Portugal,* Report no. 22391 for Petrogal, Lisboa.

Wen-Bin, D., Shu-Kun, H. & Yi-Ching, Y., 2007. A derivative-based interpretation approach to estimating source parameters of simple 2D magnetic sources from Euler deconvolution, the analytic-signal method and analytical expressions of the anomalies, *Geophys. Prospect.,* **55**(2), 255–264.

Yamada, Y. & McClay, K., 2003. Application of geometric models to inverted listric fault systems in sandbox experiments. Paper 2: Insights for possible along strike migration of material during 3D hanging wall deformation, *J. Struct. Geol.,* **25**, 1331–1336.

Zbyszewsky, G., Manupella, G., Veiga, O., Rodrigues, A. & Rodrigues, L., 1981. *Sheet 34-B, Loures, Geological Map of Portugal, 1:50,000 scale,* Geological Survey of Portugal.

Zitellini, N., Chierici F., Sartori, R. & Torelli, L., 1999. The tectonic source of the 1755 Lisbon earthquake and tsunami, *Annali di Geofisica,* **42,** 49–55.

Zitellini, N. *et al*., 2001. The 1755 Lisbon earthquake and Tsunami: localization and investigation of the tectonic source, *EOS, Trans. Am. geophys. Un.,* **82,** 290–291.